Thermal and mechanical stability of retained austenite surrounded by martensite with different degrees of tempering

Hidalgo Garcia, J.; Findley, K.O.; Santofimia Navarro, Maria

DOI
10.1016/j.msea.2017.03.017

Publication date
2017

Document Version
Final published version

Published in
Materials Science and Engineering A: Structural Materials: Properties, Microstructures and Processing

Materials Science & Engineering A 690 (2017) 337–347

Contents lists available at ScienceDirect

Materials Science & Engineering A

journal homepage: www.elsevier.com/locate/msea

Thermal and mechanical stability of retained austenite surrounded by martensite with different degrees of tempering

J. Hidalgo[a,*], K.O. Findley[b], M.J. Santofimia[a]

[a] Department of Materials Science and Engineering, Delft University of Technology, Mekelweg 2, 2628 CD Delft, The Netherlands
[b] G.S. Ansell Department of Metallurgical and Materials Engineering, Colorado School of Mines, Golden, CO, USA

ARTICLE INFO

Keywords:
Quenching and partitioning steels
Martensite tempering
Retained austenite
Thermomechanical stability

ABSTRACT

The mechanical and thermal stability of austenite in multiphase advanced high strength steels are influenced by the surrounding microstructure. The mechanisms underlying and the relations between thermal and mechanical stability are still dubious due to the difficulty of isolating other factors influencing austenite stability. In this work, martensite/austenite microstructures were created with the only significant difference being the degree of tempering of the martensite matrix. Hence, the effect of tempering in martensite is isolated from other factors influencing the stability of austenite. The thermal stability during heating of retained austenite was evaluated by monitoring phase fractions as a function of controlled temperature employing both dilatometry and magnetometry measurements. The mechanical stability was studied by performing interrupted tensile tests and determining the remaining austenite fraction at different levels of strain. The thermal stability of this remaining austenite after interrupted tests was studied by subsequent reheating of strained specimens. The results are evidence for the first time that thermal recovery of martensite during reheating assists austenite decomposition through shrinkage and softening of martensite caused by a reduction of dislocation density and carbon content in solid solution. This softening of martensite also leads to a subsequent reduction of austenite mechanical stability. Additionally, remaining austenite after pre-straining at room temperature was thermally less stable than before pre-straining, demonstrating that plastic deformation has opposing effects on thermal and mechanical stability.

1. Introduction

Multiphase steels consisting of retained austenite (RA) and martensite/bainite microstructures such as transformation induced plasticity (TRIP), low temperature bainite, and quenching and partitioning steels (Q&P) are attractive candidates for the new generation of advanced high strength steels (AHSS) [1]. These steels exhibit a remarkable combination of strength and toughness which is essential to meet the objective of weight reduction of engineering components, while maintaining the compromise of tough safety requirements. Such good mechanical properties are due to the enhanced work hardening rate caused by austenite-to-martensite transformation during deformation and the strengthening contribution of martensite/bainite.

The resistance of RA to transform into martensite upon deformation, also referred as mechanical stability, is a major factor in the mechanical response of these steels. The RA can also thermally decompose into more thermodynamically stable phases as a consequence of temperature changes, which is referred to as the thermal stability of RA. The focus of this work will be on thermal as well as mechanical stability of RA. With respect to the thermal stability of RA, this work will address the structural changes of RA during heating from room temperature and further cooling. Upon heating, austenite may transform into ferrite and carbides. Moreover, although RA might remain stable in a heating process, it can decompose into martensite during subsequent quenching. Hence, thermal stability of RA is an important issue that must be considered in the performance of the material, especially if it is subjected to processes such as welding, hot dip galvanizing, paint baking, or thermal cycling during service. Understanding the factors contributing to mechanical and thermal stability of RA is crucial for the design and processing of novel steels.

The mechanical stability of RA is dependent on chemical composition (especially the carbon and manganese content) [2–4], morphology [5,6] and grain size [5,7–9] of the austenite and the crystallographic orientation of this phase with respect to the loading direction [5]. Another important factor that is currently under review is the effect of the strength of the surrounding phase [2,3,10–14]. Xiong et al. [15] determined that austenite is mechanically more stable if it is surrounded by martensite than if it is surrounded by proeutectoid ferrite.

* Corresponding author.
E-mail address: J.HidalgoGarcia@tudelft.nl (J. Hidalgo).

http://dx.doi.org/10.1016/j.msea.2017.03.017
Received 19 November 2016; Received in revised form 3 March 2017; Accepted 5 March 2017
Available online 06 March 2017

They also suggested that carbon content of the austenite plays a secondary role in the mechanical stability of austenite. A similar result was observed by Jacques et al. [12], who referred to a mechanical 'shielding' effect of the stronger martensite during strain partitioning to explain the associated mechanical stability of austenite adjacent to martensite. Fultz et al. [11,14] suggested that the distribution of dislocations in the martensite surrounding austenite determines the capacity of martensite to plastically deform to accommodate the volume expansion accompanying austenite to martensite transformation, and thus the stability of austenite.

The thermal stability of retained austenite is mainly related to steel composition, especially carbon content [2,3]. Carbon content can have opposite effects on the thermal stability of RA during heating and cooling. Carbon enrichment of austenite is desired to stabilize this phase upon martensitic transformation during quenching, which is the premise of quenching and partitioning treatments [16,17]. On the contrary, the driving force for cementite precipitation increases with the carbon content of austenite, which can result in a higher instability of retained austenite during reheating [18]. There are also indications of a dependence of the thermal stability of RA on surrounding phases [3].

Although the mechanical and thermal stability of RA have been extensively studied, there are still some uncertainties in the factors governing them. In particular, there is not a clear link yet between thermal and mechanical stability, although there is commonality in factors that influence each, e.g. carbon content in austenite and the surrounding phases. This work focuses on the effect of martensitic microstructure characteristics on the mechanical and thermal stability upon heating of RA. Martensite/austenite microstructures were created with the only significant difference being the degree of tempering of the martensite matrix. Specifically, the dislocation density and solute carbon content of the martensite surrounding austenite were modified while maintaining a similar morphology of the martensite and volume fraction, composition and morphology of RA. Therefore, the dislocation density and carbon content of martensite are analyzed independently from other possible factors affecting stability of RA. The thermal stability of RA was evaluated by monitoring phase fractions as a function of controlled temperature employing both dilatometry and magnetometry. The mechanical stability was studied by performing interrupted tensile tests and determining the remaining austenite fraction at different levels of strain. Additionally, some specimens were reheated after interrupted tensile tests to evaluate the thermal stability of the mechanically more stable remaining austenite. Factors connecting the effect of tempering martensite on the thermal and mechanical stability of RA are proposed and discussed.

2. Experimental methods

The chemical composition of the steel used in this study is presented in Table 1. The steel was received as 4 mm thick sheets in the hot-rolled condition. Cylindrical and tensile dilatometry samples, as shown in Fig. 1a, were machined from the sheet steel along the rolling direction (RD). A Bähr DIL 805 A/D dilatometer was used to carry out different heat treatments detailed in Section 3.1 and to determine dilatometry curves in both cylindrical and tensile samples.

Resulting microstructures were resolved by scanning electron microscopy (SEM) and electron back scatter diffraction (EBSD). Specimens of each heat treatment were metallographically prepared with a final polishing step of 0.05 μm using an OPS suspension for 30 min. The SEM study was made after etching with 2% Nital, using a JEOL JSM-6500F field emission gun scanning electron microscope (FEG-SEM) operating at 15 kV. For the EBSD analysis, an Oxford Instruments Nordlys II detector mounted in the same microscope was used. The acceleration voltage was 20 kV, the beam current 1.2 nA, the working distance 25 mm, the tilt angle 70° and the step size 50 nm. Acquisition and post processing of Kikuchi patterns were performed with Oxford Instruments Channel 5 software.

Table 1
Chemical composition of the steel (wt%).

C	Mn	Si	Mo	Al	S	P	Fe
0.20	3.51	1.52	0.51	0.03	0.008	0.006	balanced

Vickers 1 kg micro hardness was measured with a Struers Durascan tester to characterize the degree of tempering of martensite after different heat treatments. X-Ray diffraction (XRD) experiments were also performed to estimate the volume fraction, lattice parameter, and dislocation density of different phases. A Bruker D8 Advance Diffractometer equipped with a Vantec position sensitive detector was employed, using Co Kα1 radiation (λ=1.78897 Å), an acceleration voltage of 45 kV and current of 35 mA, while the sample was spinning at 30 rpm. The measurements were performed in the 2θ range of 40°–130°, using a step size of 0.042° 2θ, with a counting time per step of 3 s. The volume fraction of retained austenite and the errors in determining the retained austenite fraction were calculated using the Jatczak model as described in [19]. The carbon concentration within the austenite, $\chi_{C\gamma}$, was determined from its lattice parameter a_γ, (in Å) as [20]:

$$a_\gamma = 3.556 + 0.0453\chi_C + 0.00095\chi_{Mn} + 0.0056\chi_{Al} \quad (1)$$

where χ_i, in wt%, represents the concentration of the alloying element i. Carbon concentration in martensite, $\chi_{C\alpha'}$, was calculated according to [21]:

$$\chi_{C\alpha'} = 31\cdot(a_{\alpha'} - a_\alpha), \quad (2)$$

where $a_{\alpha'}$ is the lattice parameter of martensite and a_α=2.866 Å is the lattice parameter of a reference sample. The Nelson-Riley method [22] was used to determine the lattice parameter of austenite and martensite and the modified Williamson-Hall method was used for determining dislocation density as described in [23].

Interrupted uniaxial tensile tests were carried out with the tensile specimens to evaluate the mechanical stability of retained austenite. An Instron 5500 machine was used to deform specimens up to different strains at an engineering strain rate of $6\cdot10^{-2}$ s^{-1}. Gauge deformation was measured with a contact extensometer set to have an initial span, i.e. gauge length, of 7.8 mm. The fraction of austenite remaining after interrupted tests was determined with XRD.

For the evaluation of the thermal stability of retained austenite, dilatometry and magnetometry measurements were performed during controlled temperature reheating experiments. Cubic specimens with an edge dimension of 2.0 mm for magnetic measurements were machined from dilatometry specimens. The *in situ* thermo-magnetic measurements were performed in a Vibrating Sample Magnetometer (VSM) 7307 manufactured by Lake Shore equipped with a furnace (model 73034) and calibrated with a standard NIST nickel specimen. The procedure followed is derived from the methods described in [24–26]. An austenite-free reference specimen was created by reheating the as-quenched steel to 600 °C to temper the martensitic microstructure and precipitate carbides, followed by quenching in liquid nitrogen to ensure a negligible austenite fraction in the specimen.

3. Results

3.1. Initial heat treatments and microstructures

Three different heat treatments, detailed in Fig. 1b, were selected for this work with the aim of creating microstructures consisting of martensite and retained austenite with different degrees of tempering of martensite. These heat treatments are labelled as: (a) QP, which corresponds to a Q & P treatment in which after full austenitization, the specimen is quenched to 220 °C and reheated to 400 °C for 50 s, (b) QP450, which is the QP treatment followed by tempering at 450 °C for

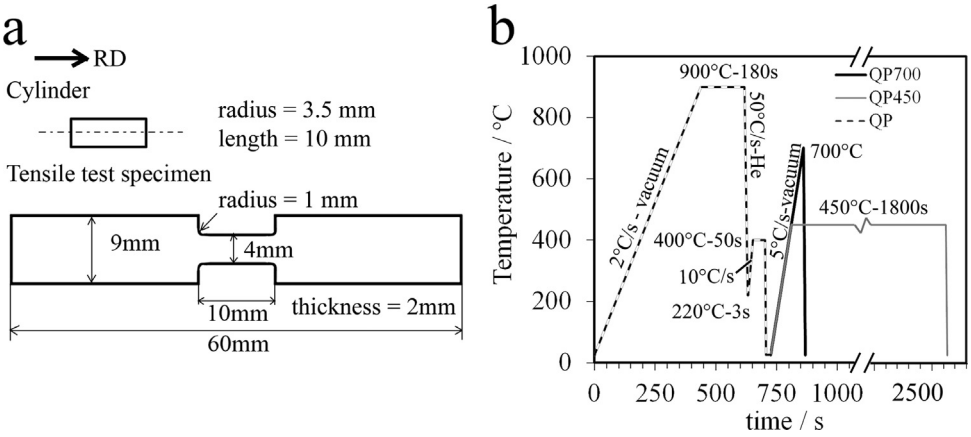

Fig. 1. (a) Dimensions of the cylindrical and tensile specimens. (b) Heat treatments applied to the steel.

1800s and (c) QP700, which corresponds to the QP treatment followed by reheating to 700 °C (just below A_{c1}=727 ± 5 °C of the material, according to previous dilatometry experiments) at 5 °C s^{-1}.

Qualitative as well as quantitative details of the microstructural evolution during the application of heat treatments were obtained from dilatometry curves and SEM micrographs as follows:

3.1.1. QP Condition

Fig. 2a shows the dilatometry curve corresponding to the Q&P heat treatment. During the first quenching, 87 ± 1 vol% of martensite was formed. This value was obtained by applying the lever rule to the dilatometry data obtained after application of a full quench from the same austenitization conditions [26,27]. A small volume expansion of 0.012% was registered during the partitioning step, showing the formation of a negligible fraction of bcc phase as a consequence of non-stationary α'/γ interfaces or austenite decomposition [28,29]. 11.5 ± 1.0 vol% of retained austenite was measured by the magnetometer after the QP treatment; thus, the fraction of fresh martensite formation during second quenching is estimated to be 1.5 ± 1.0 vol%, a fraction that is too small to be detected in the dilatometry curve. The SEM micrograph in Fig. 2b shows a microstructure consisting of lath martensite and retained austenite. Needle-type carbides grew along specific habit planes within martensite blocks substructures in the QP specimen, most likely as a result of tempering during the partitioning step.

3.1.2. QP450 condition

No indication of phase transformation was apparent in the dilatometer data during reheating after the Q&P step in QP450. The dilatometer data during reheating are shown in Fig. 2c; the change in length was due to the typical volume change associated with lattice thermal expansion. The change in length as a function of holding time at 450 °C is also shown in Fig. 2c. An increase of 0.016% in length was registered in the beginning of the isothermal holding at 450 °C, and then the length decreased continuously until the end of the holding step (Fig. 2c). The first increase in length is probably associated with a slight austenite decomposition and possible bainite formation (less than 1%), whereas further contraction may indicate carbide precipitation in the martensite or other microstructure recovery mechanisms. Somani et al. [30] suggested that at high partitioning temperatures up to 450 °C, martensite tempering competes with partitioning, which is reflected in a contraction in the dilatometry curve similar to the observations in the present paper. During quenching, there is no sign of fresh martensite formation in the dilatometry curve. Needle type carbides are vaguely distinguished in the SEM micrograph of the final microstructure in Fig. 2d; some spherical carbides are sporadically observed. Overall, the microstructure resembles that of the QP condition.

3.1.3. QP700 condition

The dilatometry data for the reheating step to 700 °C are shown in Fig. 2e. Only a slight deviation from the typical change in length associated with thermal expansion was observed around 475 °C. There are multiple mechanisms explaining this contraction that will be further discussed. In the temperature range between 675 °C and 700 °C, a slight shrinkage deviating from the ferrite thermal expansion indicates the possible formation of around 1% of austenite according to the application of the lever rule to the full ferrite to austenite transformation dilatometry curve. No sign of martensite formation is observed in the change in length curve during subsequent quenching. Spherical carbides decorating various martensite boundaries were formed in the QP700 condition as shown by the SEM micrograph in Fig. 2f.

Similar RA fractions resulted after different heat treatments as deduced from VSM measurements compiled in Table 2; the measured RA fractions were 11.2 ± 2%, 11.5 ± 2%, and 9.4 ± 2% for the QP, QP450, and QP700 conditions, respectively. These results agree with the dilatometry measurements. In Fig. 3a–c, EBSD band contrast maps combined with phase maps are shown. Blue and yellow colors correspond to bcc and fcc lattices, respectively. Part of the austenite is film-type with an elongated shape, and it is situated between martensite blocks. Block-type austenite, situated in the junction of prior austenite grains boundaries, is also visible. According to the EBSD measurements, the fraction of austenite of QP, QP450 and QP700 specimens is 0.022, 0.012 and 0.002, respectively. Subtracting these values from the total austenite fraction measured by magnetic measurements, the fraction of austenite regions having a thickness of less than 50 nm (step size of the EBSD scan) is estimated as 0.090, 0.103 and 0.092 for QP, QP450 and QP700 specimens, respectively. This austenite is assumed to be film-type. It should be noted that the EBSD maps did not cover a large region and were not considered a strong statistical representation of the volume fraction of retained austenite. However, comparing these results in the context of the present microstructures, the size and morphology of the austenite phase are considered equivalent in all specimens.

Independently of the heat treatment, the mean carbon concentration measured in RA by XRD was approximately 0.9 wt% (see Fig. 4a). The large uncertainty of the carbon concentration value comes from the high sensitivity of lattice parameter to interstitial carbon, which is affected in the same manner in all specimens by the XRD instrumental measurement error of the lattice parameter.

Therefore, it can be concluded that the applied heat treatments result in martensite/austenite microstructures with similar morphology and fraction of phases and with a similar C content in austenite. The effect of the different tempering conditions in martensite is evaluated in Section 3.2.

3.2. Degree of tempering of martensite in initial microstructures

In the previous section, differences in carbide precipitation between

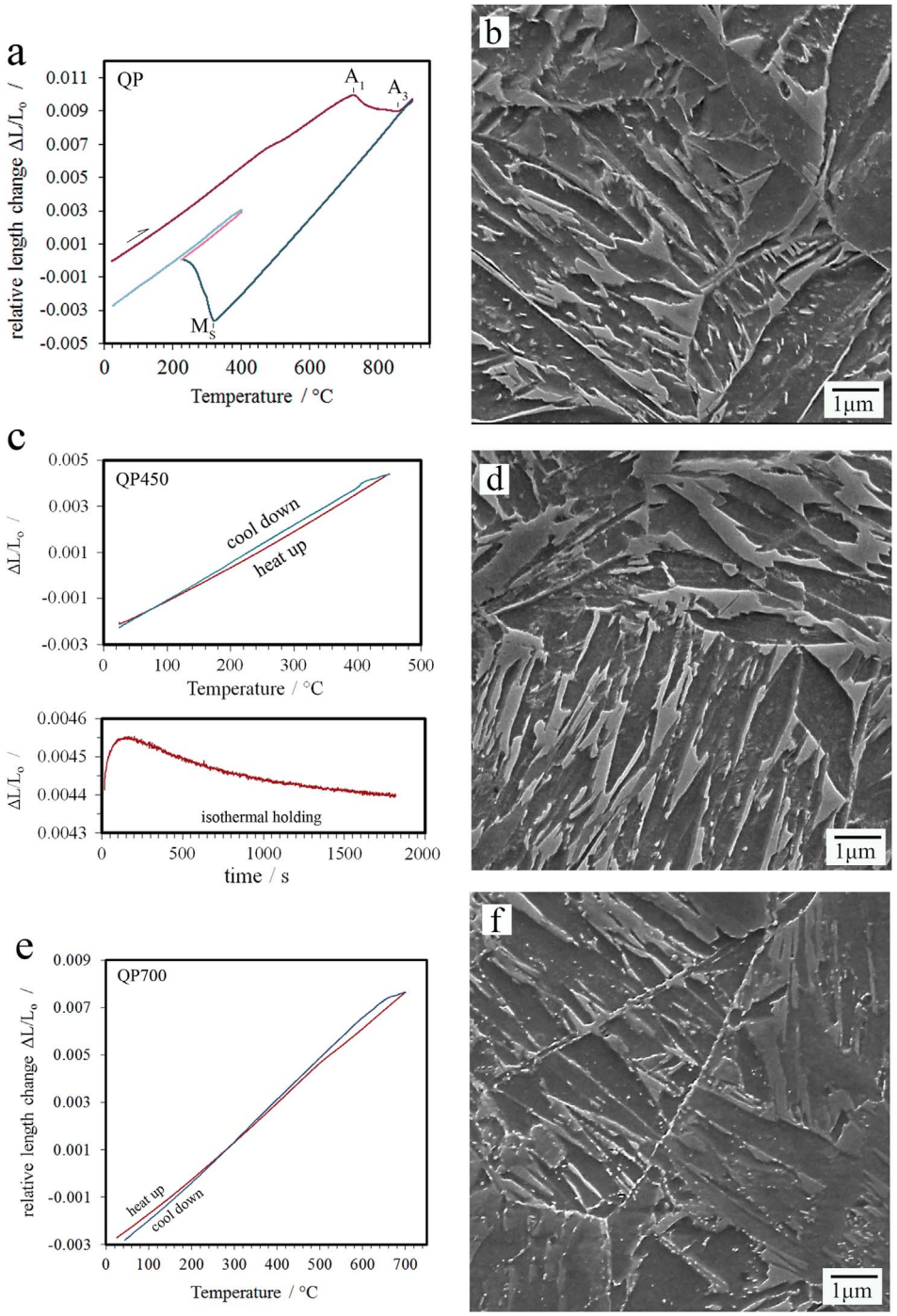

Fig. 2. Dilatometry curves of (a) QP, (c) QP450 and (e) QP700 specimens. SEM micrographs of (b) QP, (d) QP450 and (f) QP700 specimens.

Table 2
Austenite fraction calculated from VSM results for 0% and 2% strained specimens. The estimated error in determining austenite fractions is ± 1%.

	0% strained			2% strained		
$f\gamma$ /%	QP	QP450	QP700	QP	QP450	QP700
$VSM_{25\ °C}$	11.2	11.5	9.4	7.2	4.9	3.4
$VSM_{600\ °C}$	5.8	8.9	6.9	2.8	2.1	1.9

the conditions was observed, which indicates a different degree of martensite tempering. In the QP specimen, some carbon segregation to defects and carbide precipitation occurred in martensite in the absence of a tempering step. In the QP450 specimen, the holding at 450 °C and prolonged holding time likely promoted more carbon segregation in martensite and possibly partial recovery of dislocations in martensite. The recovery of dislocations and carbon segregation in martensite is expected to be most advanced in the QP700 condition during reheating to temperatures close to the intercritical region.

To evaluate the extent of the effect of different tempering conditions on the martensite microstructure, various techniques were employed:

- The carbon content and dislocation density of martensite in different specimens were evaluated by XRD. The results are shown in Fig. 4a & b. Assuming a total of 0.2 wt% C in the steel and using the measured C concentration of martensite and austenite phases weighted by their volume fraction, the carbide fraction in each

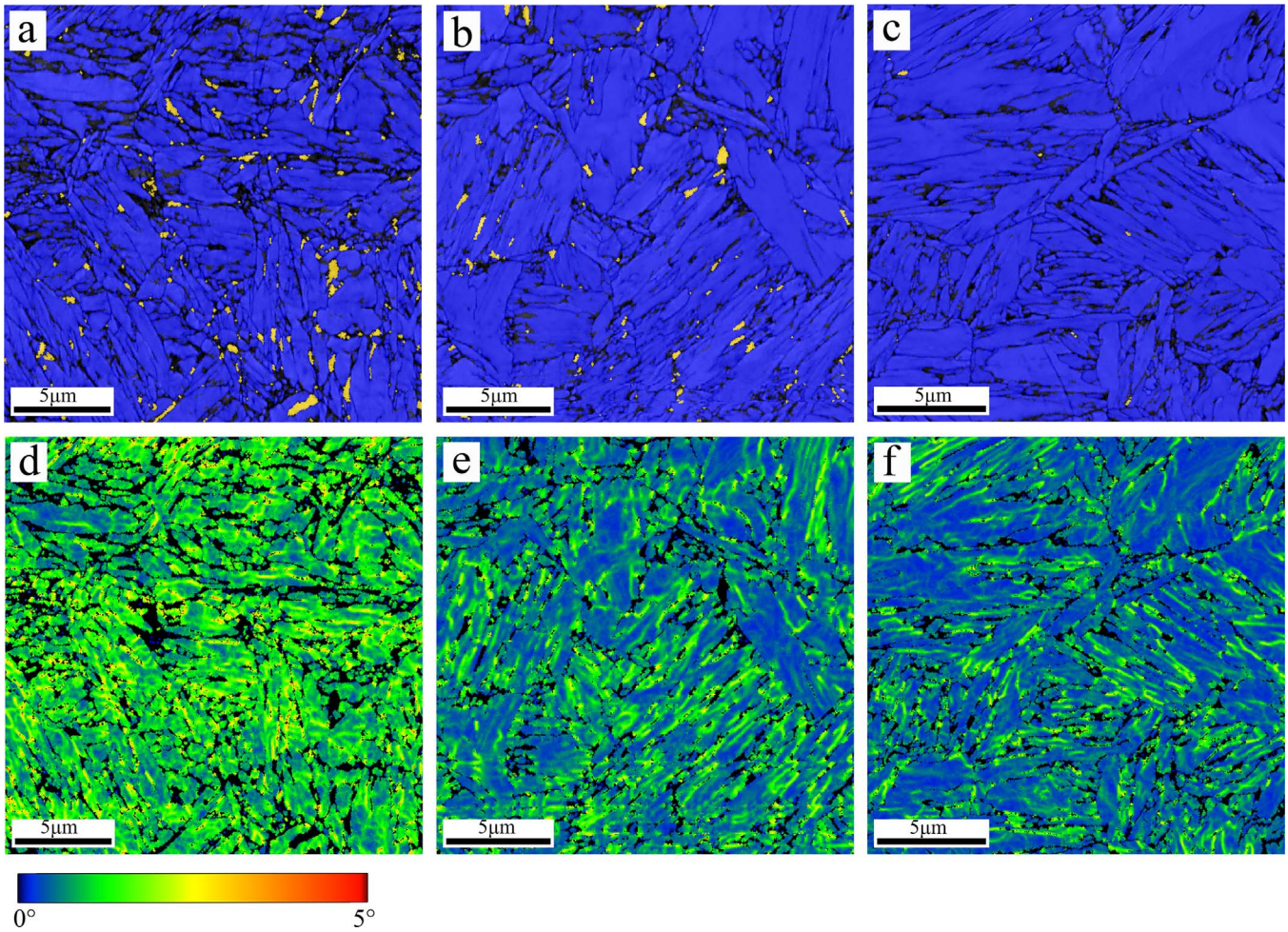

Fig. 3. EBSD maps showing (a)-(c) band contrast overimposed by phase maps, (d)-(f) kernel average misorientation maps of bcc phase. (a) and (d) QP, (b) and (e) QP450 and (c) and (f) QP700.

specimen was also calculated. The slight changes in length during isothermal holding of the QP partition stage at 400 °C, QP450 tempering stage at 450 °C, and reheating stage in QP700, suggest a fraction of bainite formation of less than 0.02 in all specimens, and thus the influence of bainite on the mass balance of carbon was neglected.

- EBSD kernel average misorientation (KAM) maps, as shown in Fig. 3d–f, were also analyzed. KAM maps indicate short-range orientation gradients within individual grains. Local changes in the lattice orientation reflect lattice curvature that can be associated with residual strain and geometrically necessary dislocations (GNDs) [31,32]. Different levels of KAM are observed within the martensite blocks in all specimens, which is indicative of the heterogeneity of strain developed through the microstructure. KAM frequency distribution curves, shown in Fig. 5, illustrate the differences between the different conditions.
- Microhardness measurements are shown in Fig. 4b. Hardness decreases as the dislocation density, also shown in Fig. 4b, and carbon content decrease in martensite, as these are the main strengthening factors.

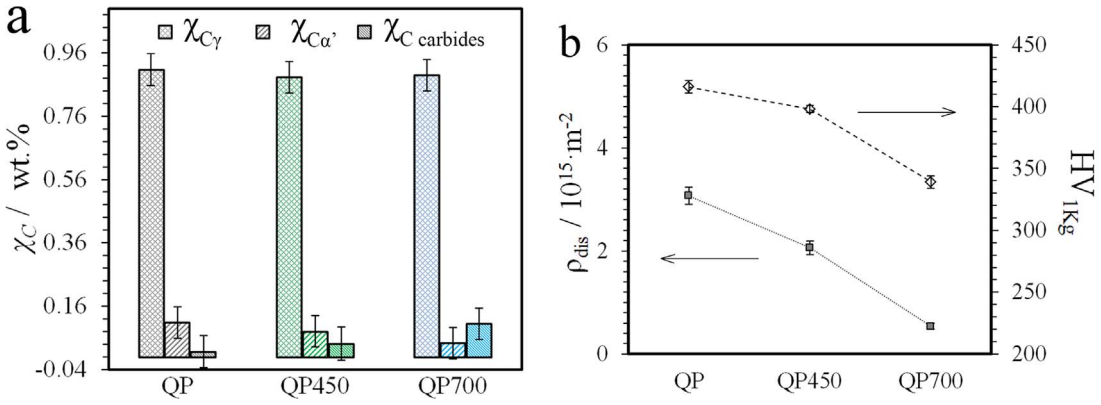

Fig. 4. (a) From left to right column: carbon concentration in austenite, martensite and reamaining C for carbide formation normalized to the total volume of phases. (b) Comparison of hardness and dislocation density.

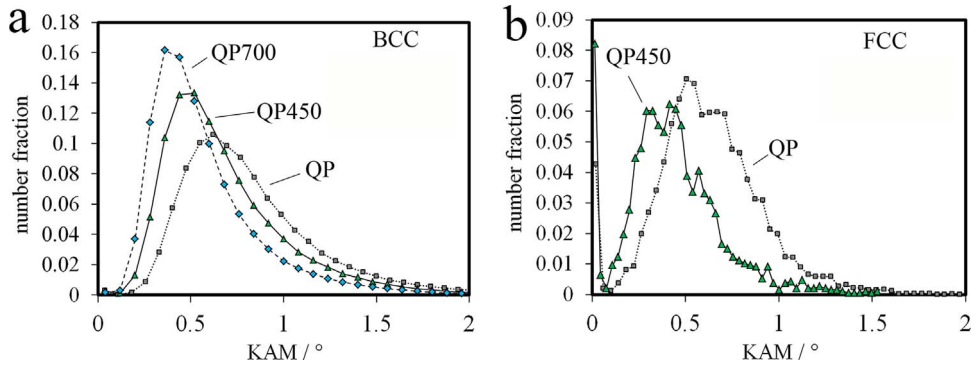

Fig. 5. Distribution of kernel average misorientation (KAM) for (a) BCC and (b) FCC phases, resulting from EBSD measurements.

Data from all of the aforementioned characterization procedures are summarized in Table 3, and are discussed next:

3.2.1. QP condition

During the partitioning step in the QP treatment, martensite partially tempers as deduced from the presence of carbides. The QP condition has the highest concentration of carbon in martensite and the lowest volume fraction of carbides of all three specimens. The high average KAM, of both austenite and martensite, reflects the high residual strain and dislocation density developed during martensite transformation in quenching. These results are supported by the highest dislocation density in martensite, measured by XRD, among all conditions and suggest that the recovery during the partitioning step at 400 °C is much less than the other heat treatment conditions. The QP condition leads to the highest hardness due to the high C content and dislocation density.

3.2.2. QP450 condition

Reheating to 450 °C for 30 min in the QP450 condition thermally affects the martensite more than QP, but not as much as in QP700. This deduction is made considering that the carbon content in martensite, estimated carbide precipitation, dislocation density, and average KAM values for QP450 were in between the QP and QP700 conditions. The less perceptible needle-type carbides in SEM micrographs (Fig. 2d) suggest carbide dissolution and eventually the start of carbide spheroidization. Part of the dissolved C may be partitioned to austenite. The hardness was reduced compared to the QP condition as a consequence of the decrease of both carbon content in solution and dislocation density in martensite. The decrease of the average KAM of austenite in QP450 specimen compared to QP specimen may be explained due to the strain recovery in martensite (also deduced from a reduction of average KAM in martensite), which would reduce the hydrostatic pressure upon the austenite phase. KAM reduction in austenite may also be a consequence of a thermally activated dislocation density recovery and reorganization of GNDs in austenite during the isothermal treatment at 450 °C.

3.2.3. QP700 condition

Martensite in QP700 specimen was the most thermally affected. The higher reheating temperature promotes carbide spherodization and growth, and dislocation recovery. This is deduced from the microstructure and the lowest solid solution carbon content in martensite, the highest fraction of carbides, and the lowest dislocation density and average KAM. This combination of factors results in the lowest hardness. The negligible fraction of austenite phase detected by EBSD did not allow the KAM value of austenite to be compared to the other conditions.

Table 3
Carbon content (χ_C), carbides, dislocation density (ρ_{dis}) and average KAM ($KAM_{Avg.}$) of martensite and HV microhardness for different specimens.

	χ_C (wt%)	Carbides (vol %)	ρ_{dis} (10^{15}. m^{-2})	$KAM_{Avg.}$ (°)	$HV_{1\ kg}$
QP	0.11 ± 0.05	0.3 ± 0.9	3.1 ± 0.5	0.797 ± 0.007	416 ± 5
QP450	0.08 ± 0.05	0.7 ± 0.9	2.1 ± 0.4	0.684 ± 0.007	398 ± 3
QP700	0.04 ± 0.05	1.8 ± 0.8	0.5 ± 0.2	0.574 ± 0.006	339 ± 5

3.3. Thermal stability of RA in initial microstructures

The thermal stability of RA in QP, QP450, and QP700 was evaluated by further reheating the specimens at 5 °C/min to 600 °C in the dilatometer and magnetometer. The resulting derivative of the change in length and the austenite fraction with temperature curves are represented together in Fig. 6. A correspondence between both curves was observed; whenever there is a remarkable change in slope in the derivative of the dilatometry curve, a detectable change in austenite fraction is observed with the magnetic measurements, which is indicated by dashed lines in Fig. 6. In the following text, these curves are interpreted and the austenite thermal stability upon heating is discussed.

3.3.1. Specimen QP

The austenite decomposes in two stages. The first stage begins at approximately 270 ± 5 °C in the magnetometer curve, which coincides approximately with an inflection in the dilatometer derivative curve followed by a plateau (indicated by first vertical dashed line from left in Fig. 6a). However, the increase in slope expected for austenite decomposition is barely observed. This can be explained by the overlap between decomposition of austenite of only 1.3 ± 1.0 vol% and precipitation of carbides, as will be contrasted later with the observation of the austenite decomposition peak in the QP700 condition. At approximately 410 ± 5 °C, the austenite fraction stabilizes with temperature. Above this temperature, an abrupt valley begins to develop in the derivative curve. The second stage of austenite decomposition begins at 475 ± 5 °C according to the magnetometer measurement, coinciding with the minimum of the derivative curve. Neglecting the effect of precipitation of carbides in the magnetic saturation, a total of 5.1 ± 1.0 vol% of austenite is decomposed at 600 °C.

3.3.2. Specimen QP450

Unlike the other conditions, austenite decomposes in a single stage in the QP450 condition. The austenite fraction remains relatively constant until 445 ± 5 °C. At this temperature, the slope of the derivative curve turns negative. The onset of this event is slightly shifted to a higher temperature and the depth of the valley is considerably lower compared to QP condition. Coinciding with the valley minimum at 485 ± 5 °C, the austenite fraction begins to decrease. A total of 3.2 ± 1.0 vol% of austenite was decomposed at 600 °C.

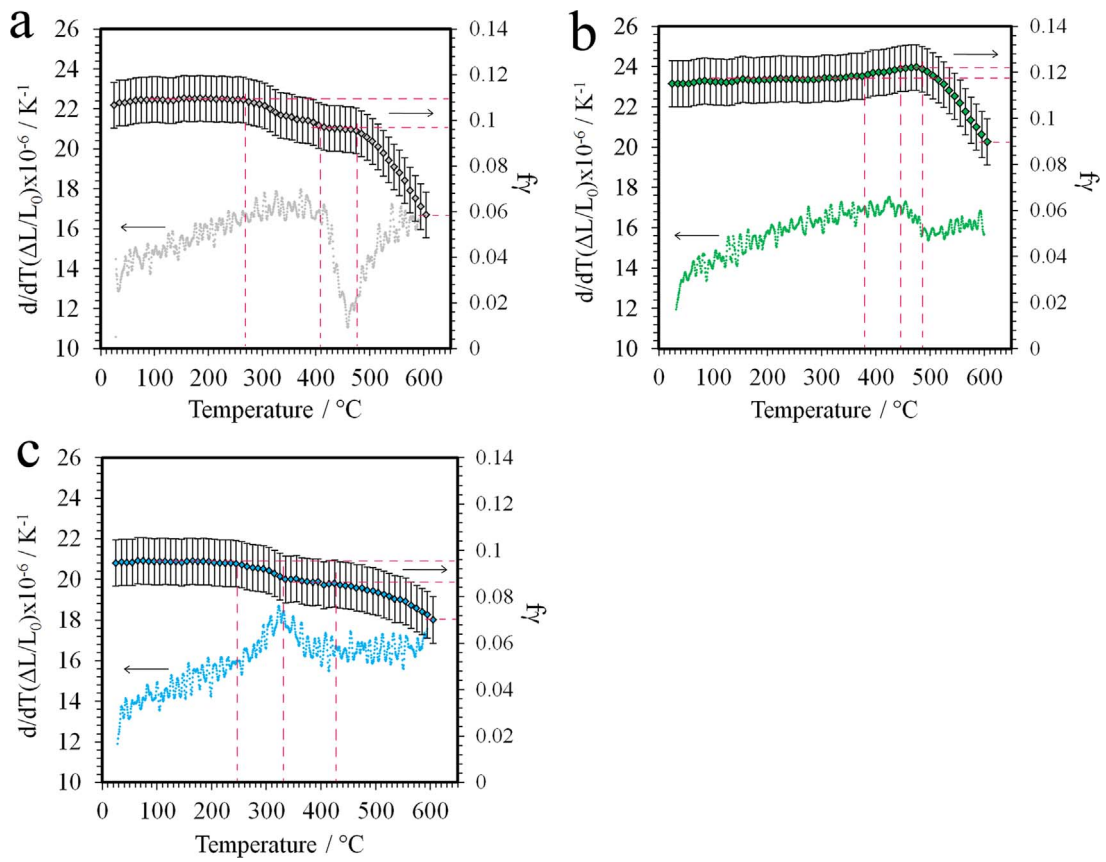

Fig. 6. Comparison of the retained austenite decomposition with temperature and derivative of change in length curves for (a) QP, (b) QP450 and (c) QP700 specimens.

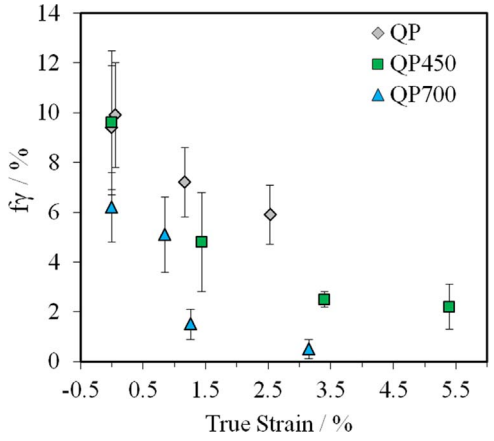

Fig. 7. Variarion of austenite volume fraction with strain. The values were obtained from XRD measurements.

3.3.3. Specimen QP700

Austenite decomposes in two stages in the QP700 condition, similar to the QP condition. In this case, the first stage begins at a lower temperature, 250 ± 5 °C, coinciding with an inflection in the derivative curve. Around 1 ± 1 vol% of austenite is decomposed, very similar to the QP condition. Austenite decomposition is more obvious in the derivative curve compared to the QP condition. An increase of slope is observed and a peak is clearly developed, with a peak maximum occurring at 330 ± 5 °C. Since a large fraction of C is assumed to have already formed carbides after the QP700 treatment according to the calculations presented in Table 3, the expansion associated with austenite decomposition upon reheating is detectable in the derivative curve since it was not offset by carbide precipitation. Precipitation of carbides in ferrite resulting from austenite decomposition is not to be discarded, which causes a negative slope in the derivative curve. Coinciding with this peak maximum, the austenite fraction stabilizes. The higher temperature tail of the derivative peak (430 ± 5 °C) is associated with the second austenite decomposition stage, at which point the austenite fraction gradually decreases leading to a total of 2.6 ± 1.0 vol% of austenite decomposed at 600 °C.

3.4. Mechanical stability of RA in initial microstructures

The evolution of the retained austenite fraction with increasing strain was determined via XRD measurements after interrupted tensile tests, and the results are shown in Fig. 7. The remaining austenite values after 2% of elongation are shown in Table 2. The decay of RA fraction moderates with strain. This decay is typical in Q & P steels and is commonly described as exponential [3,5,13].

Differences in the austenite mechanical stability are clearly observed in the different conditions. The mechanically most stable austenite is found in the QP condition with the hardest martensite, followed by QP450 and finally QP700, in which the softest martensite corresponds to the mechanically least stable austenite. As will be described below, the differences in mechanical stability are related to the degree of tempering of the martensite.

3.5. Thermal stability of the remaining austenite after straining

After interrupted tensile tests to 2% elongation, QP, QP450 and QP700 specimens were reheated at 5 °C/min to 600 °C in the magnetometer. Fig. 8a–c compare the austenite fraction evolution of strained and non-strained specimens with temperature during the heating process.

Table 2 shows the fraction of the remaining austenite at 600 °C with and without prior deformation to 2% strain.

Strained specimens shows similar evolution of austenite decom-

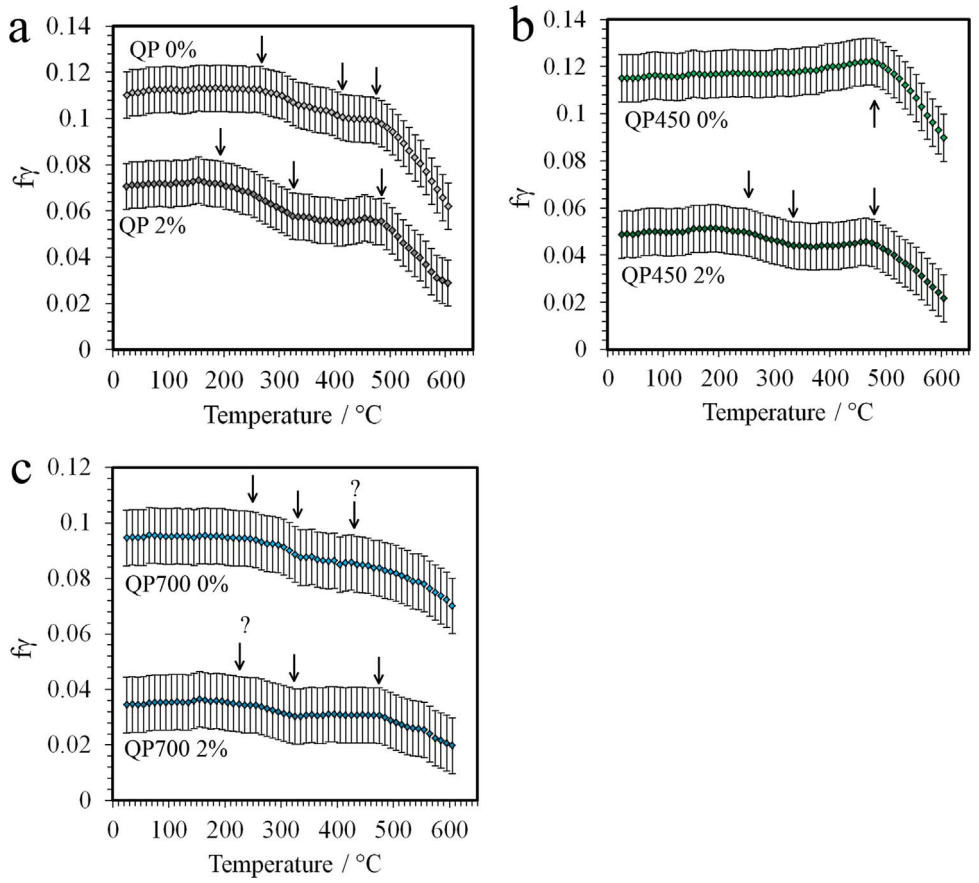

Fig. 8. Comparison of decomposition of austenite curves with temperature for 0% and 2% strained specimens (a) QP specimens, (b) QP450 specimens and (c) QP700 specimens.

position with temperature to the descriptions in Section 3.2 for non-strained specimens, except the 2% strained QP450 condition, where austenite decomposes in two stages upon subsequent reheating. The main difference is that the onset and finish of the first austenite decomposition stage, first and second arrow from left in Fig. 8 respectively, are displaced to lower temperatures in all strained conditions. The onset of the second decomposition stage, third arrow from left in Fig. 8, occurs at almost the same temperature in the strained and non-strained conditions in the case of QP and QP450. In the QP700 condition, there seems to be a shift of this onset to higher temperatures after straining.

4. Discussion

4.1. Austenite thermal stability as a function of martensite tempering

The results of Section 3.3 show that during reheating of martensite/austenite microstructures, martensite tempering facilitates austenite decomposition. The RA austenite grain size, morphology and specifically C concentration are similar in all specimens, which in principle should lead to equivalent austenite thermal stability. However, as deduced from dilatometry and magnetometry results, decomposition of austenite begins at different temperatures in the QP, QP450 and QP700 conditions. There are also variations in the fraction of austenite decomposed up to 600 °C. These differences are a result of differences in the surrounding martensite, as will be discussed in this section.

One interesting result is the observation of two austenite decomposition stages in the QP and QP700 non-strained conditions, but a single decomposition stage in the QP450 non-strained condition. Koopmans et al. [26] also observed two-stage decomposition of austenite during reheating after different Q&P treatments and the suppression of the lowest temperature stage when the partitioning time is increased. The authors hypothesized that a longer partitioning time allows better homogenization of C in austenite, leading to more uniform austenite stability. Although similar values of carbon concentration are measured in the austenite of the different specimens in the present study, heterogeneities in C concentration may exist. For example, in the QP condition, austenite regions near the interface with martensite are more likely to be more enriched in C than the interior of the grains and thus are more prone to decompose to ferrite and carbides. In the QP450 condition, the isothermal treatment for 30 min at 450 °C homogenizes the austenite C concentration, while keeping the fraction of this phase stable.

In the case of QP700 specimen, despite the higher C diffusivity at 700 °C, the relatively rapid heating may be enough to avoid complete C homogenization through austenite. The high temperatures reached promote decomposition of austenite and formation of carbides, which is shown by the lack of large austenite grains in EBSD maps and the observation of spherical carbides decorating martensite blocks and prior austenite grain boundaries. However, indication of new austenite formation is detected near 700 °C. This formation of austenite can explain the similar fraction of RA in QP700 conditions regardless of previous austenite decomposition. Freshly-formed austenite is hypothesized to grow from thermally stable film-type austenite situated between tempered martensite laths or from reverted transformation of ferrite-cementite regions [33]. Austenite forming from different sites can be another source of compositional heterogeneity that can explain the two stages of austenite decomposition in the QP700 condition.

Prior to the second decomposition stage during reheating, a sharp valley is observed in the derivative of dilatometry curve of QP condition, which decreases in size as the tempering effectiveness of QP450 and QP700 increases. This contraction deviating from thermal expansion can arise from a number of mechanisms: i) volume change due to loss of dislocation density during recovery and recrystallization

[34], ii) dissolution and spherodization of carbides, iii) precipitation of cementite and iv) relaxation of residual stresses from martensitic transformation. Indications of some of these phenomena were already observed before reheating in QP450 and to a larger extent in QP700; thus, during reheating they manifest less intensively in dilatometry results. In all conditions, the onset of the second austenite decomposition stage coincides with a change in the slope in the derivative curve, likely a result of simultaneous continued shrinkage of the tempered martensite and expansion due to austenite thermal decomposition. The onset in QP and QP450 does not differ greatly in temperature and falls within the measurement uncertainty, but is shifted to lower temperature in the QP700 condition. At temperatures higher than the onset temperature, austenite decomposes rapidly in the QP and QP450 conditions, but more gradually in the QP700 condition. In this order, the QP, QP450, and QP700 conditions go from higher to lower dislocation density and C content in martensite and from higher to lower strain heterogeneities as observed with KAM. This sequence also coincides with the sequence of decreasing austenite fraction decomposed during the second decomposition stage of austenite at high temperature during reheating. Therefore, thermal stability of RA at high temperature correlates with the previous conditions of the tempered martensite.

Assuming that there are no large differences in the carbon content of the austenite, a possible cause for the differences in thermal destabilization of austenite is softening of martensite. Because carbon segregation and dislocation recovery are most extensive in the QP700 condition before reheating, the martensite is softer than in the QP and QP450 conditions. The measured hardness differences between the conditions reflect the different degrees in martensite tempering. Hence, martensite in the QP700 condition is more prone to plastically deform to accommodate the volume expansion due to austenite decomposition explaining the shift in the initial onset of austenite decomposition to a lower temperature. In addition, martensite shrinkage due to tempering has a similar effect on austenite stability as there is a corresponding decrease in the hydrostatic pressure imposed by martensite on austenite. The lesser the degree of previous martensite tempering, the higher the shrinkage of martensite during reheating, which enhances austenite stability. The influence of these factors on RA stability are further discussed in following section.

4.2. Austenite mechanical stability as a function of martensite tempering

The hardness is the highest in the QP condition and the lowest in the QP700 condition, which show the highest and the lowest mechanical stability of austenite, respectively. Hardness can be related to the strength of the martensite, both being dependent on the solute C content and dislocation density recovery in martensite due to tempering. The solute carbon content and dislocation density in martensite are the highest in QP, followed by QP450 and QP700.

It can be assumed that with higher yield strength (YS) of martensite surrounding the austenite, there is more resistance of the martensite in accommodating the volume change accompanying the austenite to martensite transformation, increasing the stability of austenite. This interpretation has also been used to explain the effect of the phases surrounding austenite on mechanical stability of austenite TRIP steels [15].

Apart from its capacity to accommodate austenite volume expansion resulting from transformation, the surrounding martensite can influence austenite mechanical stability in other ways. During martensite formation, a hydrostatic pressure is developed within the remaining austenite particles as a result of the volume expansion associated with martensite formation. Since the volume expansion is resisted by the surrounding microstructure, there is resulting residual strain in martensite. This behavior can be seen in the KAM maps of different specimens that show large strain heterogeneities within the martensite microstructure, particularly concentrated in regions near martensite block boundaries where austenite is normally present. A high hydrostatic pressure within austenite supresses the martensitic transformation as the process requires volume expansion [2,35,36], which leads to an increase of the mechanical stability of the austenite. In the present work, the mean KAM of martensite and RA is lowered together with a reduction of the mechanical stability of austenite, from QP to QP450 and QP700 conditions, which supports the idea that the hydrostatic pressure developed within austenite particles is a factor influencing mechanical stability.

Recovery of residual strain in different conditions due to tempering is correlated with a reduction of KAM values. This process is most likely accompanied by a reorganization or coalescence of GNDs near grain boundary regions. This reorganization and coalescence of dislocations may also cause a loss of the coherence of the martensite/austenite interfaces that may favor the nucleation of martensite and thus reduce the stability of RA. Fultz et al. [11,14] discussed that the energy changes associated with the reduction of the interface coherency during tempering are rather small, and martensite nucleation is mainly influenced by the dislocation structure that forms around austenite surface. The more extended type of dislocation structure in the tempered martensite should require less formation energy to accommodate a given transformation volume, decreasing RA mechanical stability. This assertion agrees with the results of the present study and emphasizes the importance of dislocation recovery in martensite during tempering on the mechanical stability of RA.

4.3. Austenite thermal stability after strain application

The application of plastic strain during the interrupted tensile tests results in dislocation multiplication, likely in both austenite and martensite to different degrees (strain partitioning). The martensite strengthens and the dislocation structure at the interface of the untransformed austenite will change, especially if freshly formed martensite results from partially transformed austenite grains. The new freshly formed martensite likely provides an extra mechanical stabilization of RA. However the remaining untransformed austenite is less thermally stable than the non-strained conditions. Remaining austenite in QP450, which only destabilizes at high temperatures in non-strained conditions, decomposes in two stages after straining. There is also a visible increase of the austenite decomposed during the first stage in the QP condition. Additionally, the onset temperature of this first stage is shifted to lower temperatures, and thus, it is concluded that mechanisms linked to the low temperature decomposition of austenite are activated with application of strain.

Qiao et al. [37] studied the effect of cryogenic treatments on the thermal stability of austenite during subsequent tempering processes in a high carbon steel. They pointed to an increase of dislocation density in RA to explain a decrease of the thermal stability of RA at temperatures below 200 °C during heating. However, a mechanism explaining this change in stability was not provided. Fig. 9. shows that the full width half maximum (FWHM) of the {200} austenite peak broadens in all conditions after application of strain, which is an indication of a dislocation density increase. The dislocation density increase correlates with a decrease of austenite stability at low temperatures in strained specimens in agreement with the observations of Qiao et al. [37]. Due to the low intensity of austenite peaks, a reliable value of dislocation density in austenite could not be estimated by XRD. The peak broadening could also be a consequence of decreasing austenite grain size due to mechanical transformation, which also relates to mechanical strengthening.

After straining, the introduction of dislocations explains the appearance of the first austenite decomposition stage in strained QP450 condition. Defects such as dislocations and shear bands in austenite can contribute to the nucleation and formation of martensite. He et al. [38] pointed out that the pile up of GNDs at prior austenite

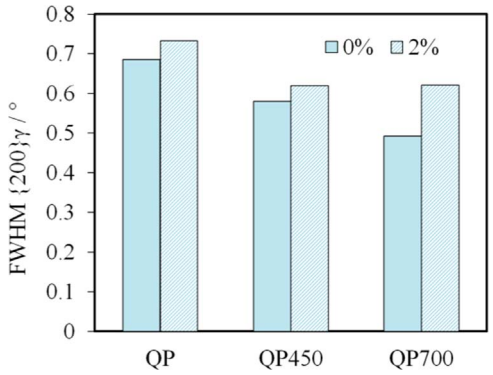

Fig. 9. Full width half maximum of the {200} austenite peak for different strained and non-strained conditions.

grain boundaries after small plastic deformation promotes the formation and development of martensite embryos, resulting in an increase of the martensite start temperature, M_S. However, at large plastic deformation the introduction of dislocation debris can mechanically stabilize the austenite due to the hindering of necessary movements of glissile martensite-austenite interfaces during transformation [39], which is reflected in a decrease of M_S. In the present study, it can be assumed that 2% deformation is not large enough to promote mechanical stabilization of austenite since at higher strains, austenite mechanical decomposition is still observed. However, the increase of dislocation density and thus de density of nucleation sites, can explain why the onset of the first decomposition stage is displaced to lower temperatures in strained specimens.

The onset of the second austenite decomposition stage occurs at approximately 480 °C in all strained conditions. This onset coincides with the non-strained condition in QP and QP450, but the onset for strained QP700 is shifted to higher temperature. This increase can be attributed to strengthening of martensite due to dislocations introduced during plastic deformation, consolidating the idea that capacity of martensite to accommodate volume expansion during austenite transformation plays a crucial role in the thermal and mechanical stability of austenite. However, these results also indicate that 480 °C is an austenite decomposition onset limit regardless of previous state of surrounding martensite. The total austenite decomposition at 600 °C is also very similar for strained and non-strained specimens. This similarity suggests that factors affecting the second stage of austenite decomposition at high temperatures are independent of the microstructure variations produced by strain, both in austenite and martensite. Most likely, high temperatures provide a more effective dislocation recovery though tempering, thus essentially generating the same microstructures in the strained and non-strained conditions.

5. Conclusions

Similar austenite/martensite microstructures were created with the only difference in dislocation density and C concentration in solution in martensite, which varied depending on the degree of tempering. From the thermal and mechanical stability studies, it was concluded that differences in the surrounding martensite influence the thermal and mechanical stability of the retained austenite:

- The austenite decomposition during reheating commonly occurs in two stages: (1) The decomposition at low temperatures is associated with heterogeneities in carbon concentration in austenite. (2) At high temperatures, the lesser the previous tempering of martensite, the higher fraction of austenite decomposed at this second stage, which suggests that thermal recovery of martensite assists the process of austenite decomposition. Shrinkage of martensite during reheating destabilizes austenite by reducing the hydrostatic pressure resisting retained austenite decomposition.
- As the dislocation density and carbon content of martensite decrease due to tempering, the strength of martensite decreases. Recovery of residual strain is shown by kernel average misorientation, most likely accompanied by a reorganization or annihilation of geometrically necessary dislocations. The recovery increases the capacity of martensite to accommodate the volume expansion of austenite transformation with strain, resulting in lower mechanical stability of austenite.
- Subsequent reheating of strained specimens shows that during the first decomposition stage remaining austenite is destabilized at lower temperatures and more transformation occurs than in non-strained conditions. This is explained by an increase of dislocation density in remaining austenite due to strain, which provides more nucleation sites for transformation. During the second decomposition stage, small differences are observed in the austenite decomposition behavior between strained and non-strained specimens, which indicates that factors affecting austenite decomposition at high temperatures are independent of microstructure variations produced by strain.

Acknowledgements

The authors want to acknowledge Jilt Sietsma, R. Huizenga and N. Geerlofs from Delft University of Technology and T. Koopmans from VDL, for their help and wise advice for the present work. The research leading to these results has received funding from the European Research Council under the European Union's Seventh Framework Programme (FP/2007–2013)/ERC Grant Agreement n. [306292]. The research also received support from support from National Science Foundation through CAREER Award No. 0955236 and the National Science Foundation/ European Research Council Research Opportunities in Europe for CAREER Awardees program.

References

[1] D.K. Matlock, J.G. Speer, Third generation of AHSS: microstructure design concepts, in: A. Haldar, S. Suwas, D. Bhattacharjee (Eds.), Microstructure and Texture in Steels, Springer, London, 2009, pp. 185–205.
[2] H. Luo Comments on "austenite stability of ultrafine-grained transformation-induced plasticity steel with Mn partitioning" by S. Lee, S.J. Lee and B.C. de Cooman, Scripta Materialia 65, 225-228, Scr. Mater. 66 (2012) 829-831, 2011.
[3] R.M. Wu, W. Li, C.L. Wang, Y. Xiao, L. Wang, X.J. Jin, Stability of retained austenite through a combined intercritical annealing and quenching and partitioning (IAQP) treatment, Acta Metall. Sin. (Engl. Lett.). 28 (2015) 386–393.
[4] Z.C. Li, H. Ding, R.D.K. Misra, Z.H. Cai, Microstructure-mechanical property relationship and austenite stability in medium-Mn TRIP steels: the effect of austenite-reverted transformation and quenching-tempering treatments, Mat. Sci. Eng.: A. 682 (2017) 211–219.
[5] D. De Knijf, C. Föjer, L.A.I. Kestens, R. Petrov, Factors influencing the austenite stability during tensile testing of Quenching and Partitioning steel determined via in-situ Electron Backscatter Diffraction, Mat. Sci. Eng. A 638 (2015) 219–227.
[6] J. Min, L.G. Hector Jr, L. Zhang, J. Lin, J.E. Carsley, L. Sun, Elevated-temperature mechanical stability and transformation behavior of retained austenite in a quenching and partitioning steel, Mat. Sci. Eng. A 673 (2016) 423–429.
[7] M.M. Wang, C.C. Tasan, D. Ponge, A. Kostka, D. Raabe, Smaller is less stable: size effects on twinning vs. transformation of reverted austenite in TRIP-maraging steels, Acta Mater. 79 (2014) 268–281.
[8] V.S.A. Challa, R.D.K. Misra, M.C. Somani, Z.D. Wang, Influence of grain structure on the deformation mechanism in martensitic shear reversion-induced Fe-16Cr-10Ni model austenitic alloy with low interstitial content: coarse-grained versus nano-grained/ultrafine-grained structure, Mat. Sci. Eng.: A 661 (2016) 51–60.
[9] R.D.K. Misra, V.S.A. Challa, P.K.C. Venkatsurya, Y.F. Shen, M.C. Somani, L.P. Karjalainen, Interplay between grain structure, deformation mechanisms and austenite stability in phase-reversion-induced nanograined/ultrafine-grained austenitic ferrous alloy, Acta Mater. 84 (2015) 339–348.
[10] C. Wang, H. Ding, M. Cai, B. Rolfe, Characterization of microstructures and tensile properties of TRIP-aided steels with different matrix microstructure, Mat. Sci. Eng.: A 610 (2014) 65–75.
[11] B. Fultz, J.I. Kim, Y.H. Kim, H.J. Kim, G.O. Fior, J.W. Morris, The stability of precipitated austenite and the toughness of 9Ni steel, Metall. Trans. A 16 (1985) 2237–2249.
[12] P.J. Jacques, F. Delannay, J. Ladrière, On the influence of interactions between phases on the mechanical stability of retained austenite in transformation-induced plasticity multiphase steels, Metall. Mater. Trans. A 32 (2001) 2759–2768.

[13] W.S. Li, H.Y. Gao, H. Nakashima, S. Hata, W.H. Tian, In-situ study of the deformation-induced rotation and transformation of retained austenite in a low-carbon steel treated by the quenching and partitioning process, Mat. Sci. Eng. A 649 (2016) 417–425.
[14] B. Fultz, J.W. Morris, The mechanical stability of precipitated austenite in 9Ni steel, Metall. Trans. A 16 (1985) 2251–2256.
[15] X.C. Xiong, B. Chen, M.X. Huang, J.F. Wang, L. Wang, The effect of morphology on the stability of retained austenite in a quenched and partitioned steel, Scr. Mater. 68 (2013) 321–324.
[16] M.J. Santofimia, L. Zhao, J. Sietsma, Overview of mechanisms involved during the quenching and partitioning process in steels, Metall. Trans. A 42 (2011) 3620–3626.
[17] J.G. Speer, E. De Moor, A.J. Clarke, Critical assessment 7: Quenching and partitioning, Mater. Sci. Tech.-Lond. 31 (2015) 3–9.
[18] A.S. Podder, I. Lonardelli, A. Molinari, H.K.D.H. Bhadeshia, Thermal stability of retained austenite in bainitic steel: An in situ study, Proceedings of the Royal Society A: Mathematical, Physical and Engineering Sciences, 467, 2011, 3141–3156.
[19] C.F. Jatczak, Retained Austenite and Its Measurement by X-Ray Diffraction, SAE Technical Papers, 1980.
[20] N.H. Van Dijk, A.M. Butt, L. Zhao, J. Sietsma, S.E. Offerman, J.P. Wright, S. Van Der Zwaag, Thermal stability of retained austenite in TRIP steels studied by synchrotron X-ray diffraction during cooling, Acta Mater. 53 (2005) 5439–5447.
[21] B. Hutchinson, J. Hagström, O. Karlsson, D. Lindell, M. Tornberg, F. Lindberg, M. Thuvander, Microstructures and hardness of as-quenched martensites (0.1-0.5%C), Acta Mater. 59 (2011) 5845–5858.
[22] J.B. Nelson, D.P. Riley, An experimental investigation of extrapolation methods in the derivation of accurate unit-cell dimensions of crystals, Proceedings of the Physical Society. 56 160-176, 1945.
[23] F. HajyAkbary, J. Sietsma, A.J. Böttger, M.J. Santofimia, An improved X-ray diffraction analysis method to characterize dislocation density in lath martensitic structures, Mat. Sci. Eng.: A 639 (2015) 208–218.
[24] L. Zhao, N.H. Van Dijk, E. Brück, J. Sietsma, S. Van Der Zwaag, Magnetic and X-ray diffraction measurements for the determination of retained austenite in TRIP steels, Mat. Sci. Eng.: A. 313 (2001) 145–152.
[25] A. Bojack, L. Zhao, P.F. Morris, J. Sietsma, In-situ determination of austenite and martensite formation in 13Cr6Ni2Mo supermartensitic stainless steel, Mater. Charact. 71 (2012) 77–86.
[26] T.T.W. Koopmans, Thermal stability of retained austenite in Quenching & Partitioning steels, in: MSc Thesis, Materials Science and Engineering Department, TU Delft: Delft, 2015.
[27] T.T.W. Koopmans, J. Sietsma, M.J. Santofimia, Analysis of the thermal stability of quenching and partitioning steel microstructures: To be published, 2016.
[28] M.J. Santofimia, T. Nguyen-Minh, L. Zhao, R. Petrov, I. Sabirov, J. Sietsma, New low carbon Q&P steels containing film-like intercritical ferrite, Mat. Sci. Eng.: A 527 (2010) 6429–6439.
[29] M.J. Santofimia, L. Zhao, J. Sietsma, Volume change associated to carbon partitioning from martensite to austenite, Mater. Sci. Forum (2012) 2290–2295.
[30] M.C. Somani, D.A. Porter, L.P. Karjalainen, R.D.K. Misra, On various aspects of decomposition of austenite in a high-silicon steel during quenching and partitioning, Metall. Trans. A 45 (2014) 1247–1257.
[31] M. Calcagnotto, D. Ponge, E. Demir, D. Raabe, Orientation gradients and geometrically necessary dislocations in ultrafine grained dual-phase steels studied by 2D and 3D EBSD, Mat. Sci. Eng.: A 527 (2010) 2738–2746.
[32] D.A. Hughes, N. Hansen, D.J. Bammann, Geometrically necessary boundaries, incidental dislocation boundaries and geometrically necessary dislocations, Scr. Mater. 48 (2003) 147–153.
[33] R. Wei, M. Enomoto, R. Hadian, H.S. Zurob, G.R. Purdy, Growth of austenite from as-quenched martensite during intercritical annealing in an Fe-0.1C-3Mn-1.5Si alloy, Acta Mater. 61 (2013) 697–707.
[34] H. Azizi-Alizamini, M. Militzer, W.J. Poole, Austenite formation in plain low-carbon steels, Metall. Trans. A 42 (2011) 1544–1557.
[35] G.K. Tirumalasetty, M.A. van Huis, C. Kwakernaak, J. Sietsma, W.G. Sloof, H.W. Zandbergen, Deformation-induced austenite grain rotation and transformation in TRIP-assisted steel, Acta Mater. 60 (2012) 1311–1321.
[36] N. Nakada, Y. Ishibashi, T. Tsuchiyama, S. Takaki, Self-stabilization of untransformed austenite by hydrostatic pressure via martensitic transformation, Acta Mater. 110 (2016) 95–102.
[37] X. Qiao, L. Han, W. Zhang, J. Gu, Thermal stability of retained austenite in high-carbon steels during cryogenic and tempering treatments, ISIJ Int. 56 (2016) 140–147.
[38] B.B. He, W. Xu, M.X. Huang, Increase of martensite start temperature after small deformation of austenite, Mat. Sci. Eng.: A. 609 (2014) 141–146.
[39] S. Chatterjee, H.S. Wang, J.R. Yang, H.K.D.H. Bhadeshia, Mechanical stabilisation of austenite, Mater. Sci. Tech. Ser. 22 (2006) 641–644.